JOURNAL OF GEOPHYSICAL RESEARCH, VOL. 112, A12213, doi:10.1029/2006JA012138, 2007

Loss of relativistic electrons: Evidence for pitch angle scattering by electromagnetic ion cyclotron waves excited by unstable ring current protons

M. Sandanger,[1] F. Søraas,[1] K. Aarsnes,[1] K. Oksavik,[2] and D. S. Evans[3]

Received 25 October 2006; revised 16 August 2007; accepted 27 September 2007; published 22 December 2007.

[1] During geomagnetic storms the flux of radiation belt electrons can increase, decrease, or stay constant, depending on the competition between acceleration and loss mechanisms. We focus on loss of relativistic electrons. We use low-altitude polar-orbiting spacecraft and analyze fluxes of tens to hundreds of keV protons and relativistic (>1.5 MeV) electrons during a moderate geomagnetic storm, with a long-lasting recovery phase (4–5 d). Using data from four local times, we find that the loss of relativistic electrons is confined within the anisotropic proton zone and that a spatially limited loss of relativistic electrons is spatially collocated with increased loss of protons. The proton pitch angle distributions within these peaks are consistent with moderate to strong pitch angle scattering due to electromagnetic ion cyclotron (EMIC) waves. The loss of relativistic electrons collocated with protons is found at all four local times considered (0300, 0700, 1400, 1700 MLT). Since anisotropic proton distributions can under certain conditions generate EMIC waves, we find strong indications that the observed relativistic electrons are scattered into the atmospheric loss cone by EMIC waves. EMIC wave scattering is less efficient at high equatorial pitch angles but very efficient near the loss cone, thereby controlling the loss rate of relativistic electrons to the atmosphere. Our observations in and near the loss cone support theoretical work suggesting that EMIC waves can cause scattering loss to the atmosphere of relativistic electrons over the course of a geomagnetic storm.

Citation: Sandanger, M., F. Søraas, K. Aarsnes, K. Oksavik, and D. S. Evans (2007), Loss of relativistic electrons: Evidence for pitch angle scattering by electromagnetic ion cyclotron waves excited by unstable ring current protons, *J. Geophys. Res.*, *112*, A12213, doi:10.1029/2006JA012138.

1. Introduction

[2] The outer radiation belt consists of 0.4–15 MeV electrons on fairly stable orbits [*Li and Temerin*, 2001]. Geomagnetic storms can decrease or increase the fluxes of relativistic electrons. *Reeves et al.* [2003] investigated the dynamics of the outer radiation belt by examining 276 moderate and intense storms during a full solar cycle. They found that only about half of the storms increased the fluxes of relativistic electrons, one quarter decreased the fluxes, and one quarter gave little or no change. Whether a geomagnetic storm increases or decreases the fluxes of relativistic electrons in the outer radiation belt is determined by competing acceleration and loss mechanisms. The scientific issues surrounding the acceleration and loss of relativistic electrons present a number of interesting questions that have not yet been fully resolved (e.g., see the review by *Friedel et al.* [2002]). During geomagnetic storms, whistler mode waves are excited by electron temperature anisotropies which develop as electrons convect inward from the plasma sheet, and these waves can energize electrons from $\leq$100 keV up to MeV energies [*Horne and Thorne*, 1998; *Horne et al.*, 2003, 2005a, 2005b]. A recent study showed that whistler mode wave acceleration might be a dominant mechanism for the acceleration of MeV electrons [*Shprits et al.*, 2006a]. *Summers et al.* [1998] proposed a model to account for the flux variation of relativistic electrons during geomagnetic storms by combining resonant interaction with whistler-mode chorus outside the plasmasphere and pitch angle scattering by electromagnetic ion cyclotron (EMIC) waves in the evening MLT sector inside the plasmasphere. *Summers and Ma* [2000] and *Summers et al.* [2004] showed that relativistic electron generation in the outer zone by chorus diffusion is effective during a storm with a long-lasting recovery phase over which many substorms occur, or during high-intensity long-duration continuous AE activity (HILDCAA) events. *Meredith et al.* [2003a] carried out a statistical analysis of over 800 EMIC wave events and concluded that EMIC wave scattering could significantly affect relativistic electron dynamics during a storm. The waves that resonated with the

[1]Department of Physics and Technology, University of Bergen, Bergen, Norway.
[2]Johns Hopkins University Applied Physics Laboratory, Laurel, Maryland, USA.
[3]NOAA Space Environment Center, Boulder, Colorado, USA.

0148-0227/07/2006JA012138$09.00

MeV electrons were produced by low-energy (tens of keV) ring current protons, which are injected into the inner magnetosphere during enhanced convection/substorm events. In this paper we focus on geomagnetic storms with loss of relativistic electrons into the atmospheric loss cone due to pitch angle scattering by EMIC waves.

[3] Early theoretical studies by *Thorne and Kennel* [1971] and *Lyons and Thorne* [1972] considered the process of resonant pitch angle scattering of relativistic electrons by EMIC waves during the main phase of a geomagnetic storm. *Joselyn and Lyons* [1976] investigated the pitch angle distributions of ring current protons in the *L*-region 3–5 during the recovery phase of a large geomagnetic storm. They found the observed proton energy spectra and pitch angle distributions to be sufficient to amplify ion cyclotron waves throughout the whole *L*-region. Loss of relativistic electrons due to EMIC waves is further investigated by *Albert* [2003]. The loss involves resonant pitch angle scattering of relativistic electrons throughout the region of intense ring current generated ion-cyclotron turbulence. *Summers and Thorne* [2003] found that relativistic electrons can, under certain conditions, be removed from the outer radiation belt by EMIC wave cyclotron resonant scattering over a timescale of several hours to a day. Electron minimum resonant energies of less than 2 MeV are restricted to regions of high plasma density and/or weak magnetic field, where $\omega_{pe}/\omega_{ge} \geq 10$ and ω_{pe} and ω_{ge} are the electron plasma frequency and electron gyrofrequency, respectively [*Meredith et al.*, 2003a]. This is typically satisfied in the duskside plasmapause or in the regions of plumes. The free energy for the cyclotron instability is the anisotropic pitch angle distribution of ring current protons. The instability causes pitch angle diffusion, proton precipitation, and generation of ion cyclotron waves. *Engebretson et al.* [2007] analyzed Cluster observations of Pc 1–2 waves and associated ion distributions during two large geomagnetic storms in 2003. Owing to their observations they suggested that ion cyclotron wave growth rates could be significantly increases by addition of cool hydrogen. *Lundblad and Søraas* [1978] reported regions of enhanced proton precipitation in connection with SAR (stable auroral red arc) formation, thereby supporting the *Cornwall et al.* [1971] theory that ion cyclotron waves generate the SAR arc. The observational study by *Søraas et al.* [1999] further supports the view that enhanced ion precipitation at midlatitudes is caused by cyclotron wave-particle interactions. During the storm main phase they found regions of enhanced precipitation in the midnight/afternoon sector, and in the storm recovery phase enhanced proton losses were found in the morning sector. *Søraas et al.* [1980] found that IPDP (irregular pulsations with diminishing periods) were related to the injection of protons during substorms. *Jordanova et al.* [1996] modelled ring current proton precipitation due to EMIC wave scattering, and found that maximum precipitation occurs within regions of maximum EMIC wave instability. *Yahnina et al.* [2003] analyzed NOAA-12 (National Oceanic and Atmospheric Administration) spacecraft data to observe enhanced energetic midlatitude particle precipitation simultaneous with ground-based Pc1 and IPDP observations and concluded that these regions were the particle counterparts of EMIC wave activity. *Yahnina et al.* [2003] confirmed that the plasmapause is a preferred region for generation and propagation of EMIC waves in the Earth's magnetosphere.

[4] Ion-cyclotron waves generated by unstable ring current protons could play a significant role in the loss of relativistic electrons in the outer radiation belt. In order to carry out an experimental investigation of the correspondence between the loss of relativistic electrons and EMIC waves, we study the spatial correspondence between the loss of relativistic electrons and the loss of protons, the particle counterparts of EMIC wave activity.

[5] The main focus will be on the relationship between relativistic (>1.5 MeV) electrons and 30–80 keV protons. An example of such a spatial correspondence was shown in the work of *Søraas et al.* [2005]. In section 2 we briefly describe the satellite instrumentation used in this study. A detailed examination of some selected satellite passes will be presented in section 3. In section 4 an overview of the energetic particle environment during a moderate geomagnetic storm is presented. In section 5 we present our summary and discussions, and in section 6 we present the conclusions.

2. Instrumentation

[6] The NOAA spacecraft have a polar orbit at around 815 km altitude. Each orbit takes about 103 min. During the year 1998 the approximate local time ascending node equatorial crossing for NOAA-12 is 1700 MLT. Figure 1 gives a sketch of the spacecraft orbit (dashed line). *Raben et al.* [1995] describe the spacecraft and instrumentation.

[7] The present study uses observations of protons and electrons from the Medium Energy Proton and Electron Detector (MEPED) and the omnidirectional detector (dome) on board NOAA-12. Particle data from these detectors on board the NOAA-14 (similar to the one on board NOAA-12) have been used to confirm the behavior of the particles at 0300 and 1400 MLT but is not shown in this paper. The MEPED instrument measures protons and electrons at angles of 10deg and 90deg with the local vertical and with an opening angle of ±15deg Full Width Half Maximum (FWHM). Figure 1 illustrates the NOAA-12 orbit and viewing angle of the horizontal and vertical MEPED telescope detectors at around 60deg ILAT. The protons are measured in five energy bands from 30 to 2500 keV, and electrons in the integral channels >30, >100, and >300 keV. The omnidirectional dome instrument looks in the same direction as the vertical MEPED telescope detector and consists of a three element telescope (P6, P7, and P8) with an opening angle of ±60deg FWHM. The detectors measure in respectively three integral channels detecting protons at energies >16, >36, and >80 MeV. The P6 detector also responds to electrons with energies above 800 keV as well as >16 MeV protons. The response function (efficiency) of the detector reaches a value of around 0.5 when the incident electron energy is close to 1.5 MeV and 1 for electrons above 2 MeV (T. Cayton, private communication, 2003). In other words, half of the incident electrons with energy of 1.5 MeV are detected. It is only during solar proton events that the electron measurements in the *L* range 3–5 can be contaminated by protons >16 MeV, and such events are deleted form our studies.

[8] In the *L* range 3–7 the atmospheric loss cone at the satellite altitude varies from 58.9deg to 59.9deg, assuming that the particles are lost at 110 km altitude. The observing direction of the vertical detector in this *L*-range in the

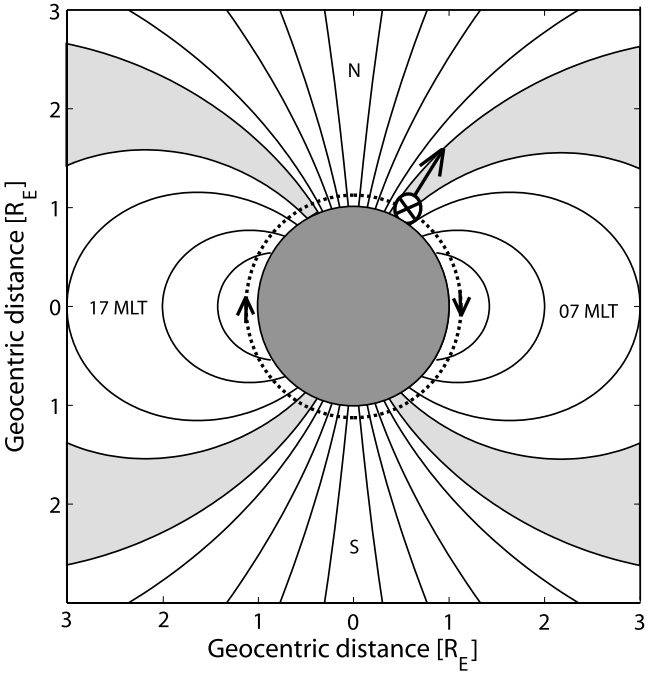

Figure 1. NOAA-12's orbit relating to the Earth's magnetic field and the direction of the vertical and horizontal detectors. At high latitudes (>50deg) the vertical detector looks approximately along the magnetic field and around the equator it looks normal to the magnetic field. The horizontal detector, however, looks normal to the magnetic field during the whole orbit.

Northern Hemisphere is between 10.8deg and 19.9deg with respect to the local magnetic field and with an opening angle of ±15deg FWHM the measured particles are well inside the loss cone. The observing direction of the horizontal detector in the same *L*-region varies between 88.5deg and 90.5deg with respect to the local magnetic field. With an opening angle of ±15deg FWHM the detector measures particles mirroring above 600 km altitude. The observing direction of the dome detector in the *L* range 3–7 in the Northern Hemisphere is between 10.8deg and 19.9deg. With an opening angle of ±60deg FWHM the dome detector will mostly measure particles inside and at the edge of the atmospheric loss cone.

[9] In other words, when the spacecraft is at high latitudes, the horizontal detector will measure particles just outside the loss cone, and the vertical detector will measure in the central part of the loss cone. The dome instrument measures particles that are mostly inside the loss cone.

3. Low-Altitude Observations of Ring Current Protons and Relativistic Electrons During Individual Passes

[10] Figure 2 exhibits data from the morning sector measured by NOAA-12. The pass was during the recovery phase of a storm to be discussed below. The pass starts in the northern polar cap at MLT ~1800 and pass over to the morning side auroral oval at MLT 0600 and goes via the equator into the southern morning auroral oval and into the polar cap. Figure 2a displays precipitating (well into the loss cone) electrons >30 keV (solid line), and locally mirroring (at the edge of the loss cone) electrons >30 keV (dashed line), while Figure 2b shows precipitating relativistic electrons. Owing to the 60deg opening angle of the dome detector these electrons are within and on the edge of the loss cone. Figure 2c shows precipitating (well into the loss cone) 30–80 keV protons (solid line) and locally mirroring (at the edge of the loss cone) 30–80 keV protons (dashed line). The isotropic poleward zone has equal fluxes of protons along and normal to the magnetic field, while the equatorward anisotropic zone has a very reduced flux along the magnetic field. The locally mirroring protons in Figure 2c exhibit, however, two clear midlatitude enhancements. Such midlatitude enhancements are typical for the storm recovery phase and indicates increased pitch angle scattering [*Lundblad and Søraas*, 1978; *Søraas et al.*, 1999; *Yahnina et al.*, 2003]. The relativistic electron precipitation (Figure 2b), in both hemispheres, starts immediately equatorward of the isotropic proton boundary and is confined within the region of anisotropic protons (Figure 2c). The anisotropic proton zones in the two hemispheres are actually almost identical. The structure in the relativistic electron precipitation is observed to be similar to the structure in the protons, both exhibiting a pronounced equatorward peak and a smaller peak at higher latitudes. In particular the equatorward peak in the Southern Hemisphere is worthy of notice. Here the loss of relativistic electrons increases by more than an order of magnitude in a narrow spatial region (20 km at the height of the spacecraft). This increased loss of high-energy electrons is collocated with the marked increase in the losses of 30–80 keV protons. In the Northern Hemisphere the relativistic electrons and the protons also exhibit coincident peaks. The population of >30 keV electrons in Figure 2a shows no direct spatial correspondence with the populations of protons or the relativistic electrons, and they also extend to much lower latitudes.

[11] Figures 3 and 4 show additional comparisons between the relativistic electrons and protons. NOAA-12 measurements from 1615 to 1705 UT (morning 0600 MLT) on day 207 are displayed in Figures 3a–3b. Measurements from 1323 to 1413 UT (evening 1700 MLT) on the following day are displayed in Figures 3c–3d. Similar measurements from 1215 to 1305 UT (evening 1700 MLT) on day 202 and 0700–0751 UT (evening 1700 MLT) on day 207 are displayed in Figures 4a–4b and Figures 4c–4d, respectively.

[12] Figure 3 confirm the pattern shown in Figure 2. The observations in the two hemispheres are closely conjugate, and both the relativistic electrons and protons exhibit collocated enhancements. It should be emphasized that NOAA-12 makes observations at different magnetic field strengths as the magnetic longitude and latitude changes throughout the orbit. The difference in magnetic field strength can to a large extent account for differences in intensity in the particle flux between hemispheres. In Figures 2 and 3 the observations of the protons and the relativistic electrons in one hemisphere are more or less a mirror image of the observations in the other hemisphere, even though the observations are 30 min apart. This implies that the phenomena are stable and long-lasting. Having examined numerous similar plots, we find that the same picture emerges, namely that the relativistic electron loss is always within the region of anisotropic proton

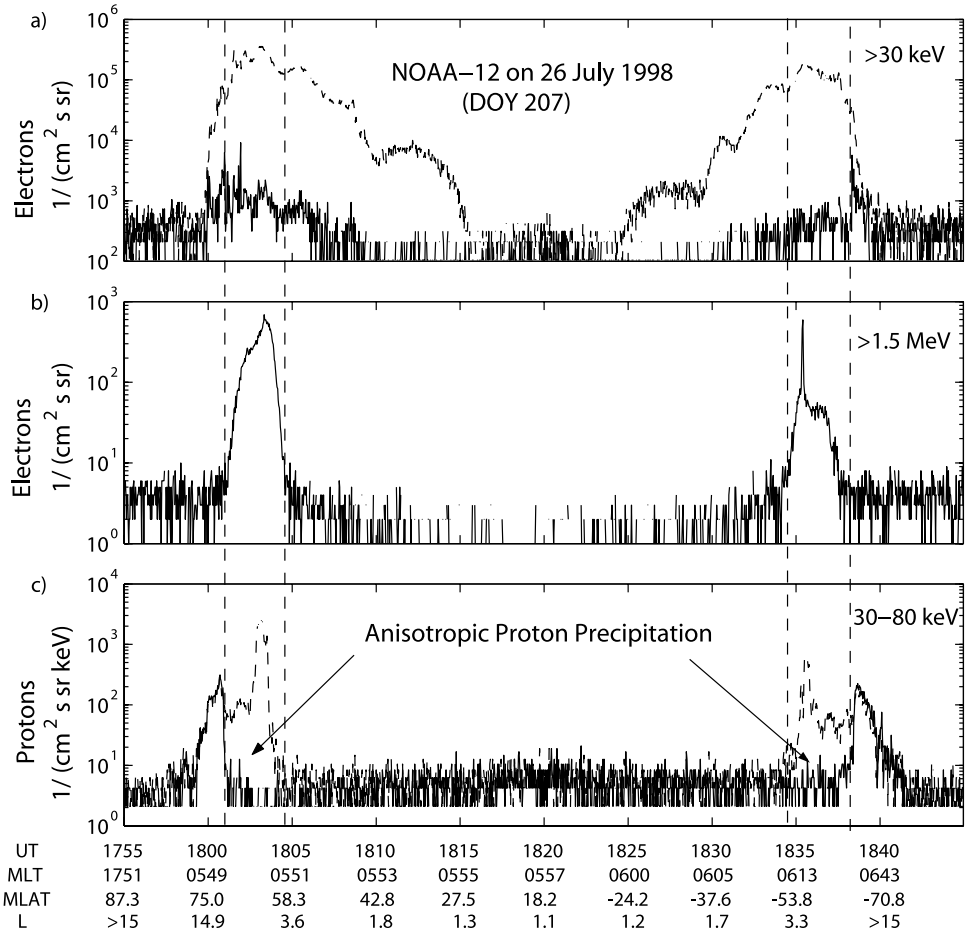

Figure 2. Particle data from a pole-to-pole morning side orbit by NOAA-12 on 26 July 1998. From the top is shown electrons >30 keV, from both the 0deg (solid line) and 90deg (dashed line) MEPED detectors, electrons >1.5 MeV measured by the dome detector, and 30–80 keV protons, measured by the 0deg (solid line) and 90deg (dashed line) MEPED detectors. The dashed vertical lines delimit the anisotropic proton zone.

flux, and peaks in the proton data are collocated (or near collocated) with peaks in the loss of relativistic electrons. The structure of the anisotropic proton flux tracks the structure of the relativistic electron precipitation; peaks in the anisotropic proton flux correspond to similar peaks in the relativistic electron precipitation. These peaks thus indicate increased coincident losses/pitch angle scattering for both particle species.

[13] In the observations shown in Figures 2 and 3 no increased intensity in the vertical proton detector is evident. A quite possible explanation is that weak pitch angle scattering does not scatter the protons deep enough into the loss cone to be detected by the vertical proton detector. There are however cases where the intensity in the vertical detector also are greatly enhanced. Figures 4b and 4d show intense spikes in both the horizontal and vertical proton detector located inside the anisotropic proton zone in the northern hemisphere (to the right). These proton spikes indicate very strong pitch angle scattering and complete filling of the loss cone. We can observe collocated peaks in the loss of relativistic electrons in Figures 4a and 4c.

[14] The loss of relativistic electrons is almost always inside the anisotropic proton zone. The Southern Hemisphere in Figure 4 exhibit an exception as the region of relativistic electron losses extend into the isotropic proton zone. One possible explanation can be found by looking at the Northern Hemisphere. The precipitation in the Northern and Southern Hemisphere are usually almost mirroring images of each other. The spikes in the Northern Hemisphere are close to the isotropic proton zone. In the Southern Hemisphere the proton spikes seem to have merged with the isotropic proton zone resulting in a continuous isotropic proton precipitation.

4. Overview of the 20–29 July 1998 Storm

[15] Figures 5a–5d show NOAA-12 particle data from 20 to 29 July 1998 displayed with a logarithmic color scale, plotted versus ILAT and UT with 14 passes each day. From Figure 5e it is seen that early in day 202 there is a sudden commencement (SC) which is followed by a decrease in Dst to −10 nT. Late in day 203 there is a new SC followed by a minor storm, Dst decreasing to −45 nT. The storm is associated with a high-speed solar wind stream reaching a speed of 700 km/s, shown in Figure 6a. The storm has a slow recovery, taking almost five days to reach a quiet level, and it is associated with a high-intensity long-duration

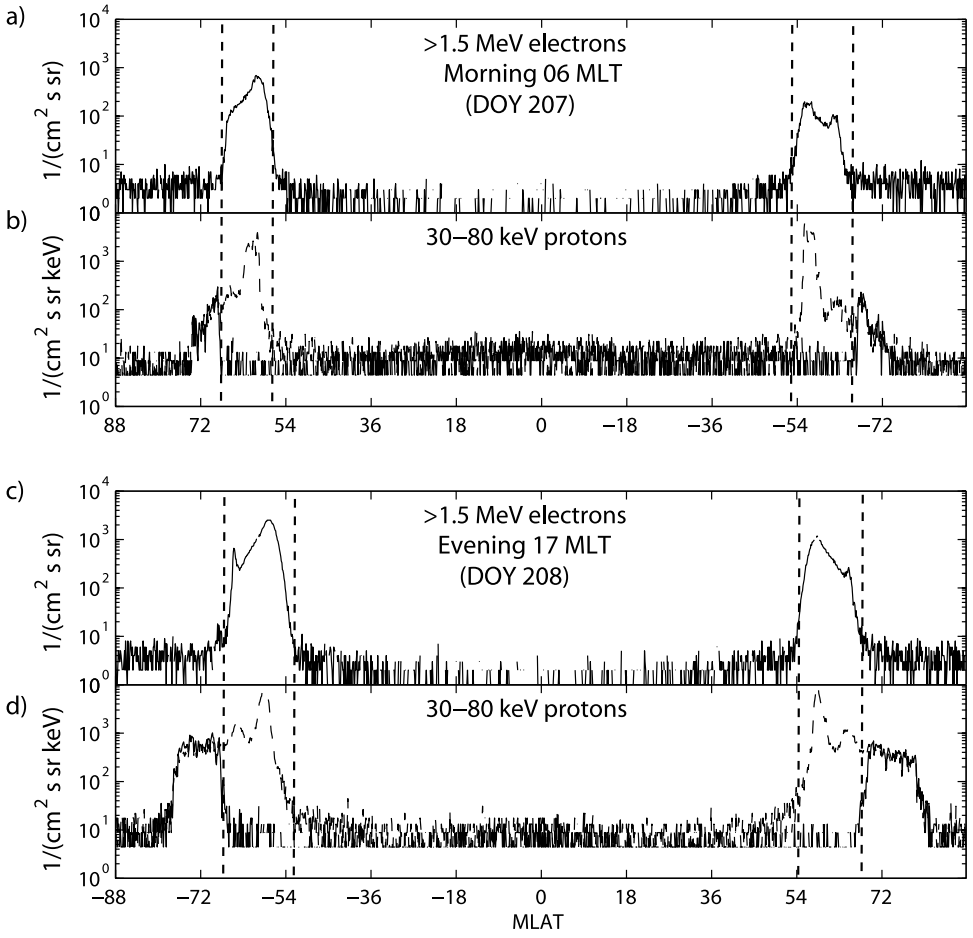

Figure 3. Particle data from NOAA-12 on 26 and 27 July 1998. The figure exhibits electrons >1.5 MeV and protons 30–80 keV, from the 90deg (dashed line) and 0deg detectors (a and b) from a morningside pole-to-pole orbit on 26 July (1615–1705 UT), and (c and d) from an eveningside pole-to-pole orbit on the next day (1323–1413 UT).

continuous AE activity (HILDCAA) event [*Tsurutani and Gonzalez*, 1987]. *Søraas et al.* [2004] and *Sandanger et al.* [2005] have shown that during HILDCAA events there is an ion injection into the outer part of the ring current delaying its recovery. HILDCAA events are known to be associated with relativistic electrons [*Meredith et al.*, 2003b; *Summers et al.*, 2004; *Horne et al.*, 2006]. Whistler mode turbulence is a strong candidate for the generation of relativistic electrons in the region $3 < L < 5$ during magnetic storms with a several-day recovery phase [*Summers et al.*, 1998; *Summers and Ma*, 2000].

[16] In Figure 5a a small increase is seen in the precipitating protons during day 202 and a major one on 204 when Dst reached values of −10 and −45 nT, respectively. The proton precipitation measured by the vertical detector extended equatorward to ILAT 62deg and 60deg during these 2 d. The isotropic proton precipitation on the nightside is a measure of proton injection into the ring current/radiation belt [*Søraas et al.*, 2002]. After the two particle injections, on day 202 and 204, there is a gradual decrease in the proton injection and it only involves the outer part (ILAT > 65deg) of the ring current during the storm recovery phase.

[17] In Figure 5b the behavior of the locally mirroring protons is shown. In the poleward part, the intensity of the locally mirroring protons is the same as that of the field-aligned protons, giving rise to an isotropic pitch angle distribution. Equatorward of this region the locally mirroring protons dominate, giving rise to a region with anisotropy. The size of the anisotropic region increases during the storm recovery, and exhibit patches indicating localized flux enhancements, as the peaks shown in Figures 2, 3, and 4. The pitch angle distribution within these peaks is consistent with moderate to strong pitch angle scattering.

[18] In Figure 5c the color-coded logarithm of the ratio between the locally mirroring protons and the precipitating protons is shown. The inserted black lines indicate the latitude extent of the anisotropic proton zone, which is where the ratio exceeds 10. The upper blue color indicates the isotropic poleward zone.

[19] Figure 5d shows the relativistic electrons with energies >1.5 MeV measured by the dome instrument. The relativistic electrons are present on day 201 before the first SC, in the recovery phase of a previous storm. Then they decrease during day 203 and stay depressed well into the recovery of the storm. On day 205 they reappear and exhibit increasing intensity during the recovery phase of the storm. The relativistic electrons are almost entirely within the region where the proton anisotropy exceeds a ratio of 10,

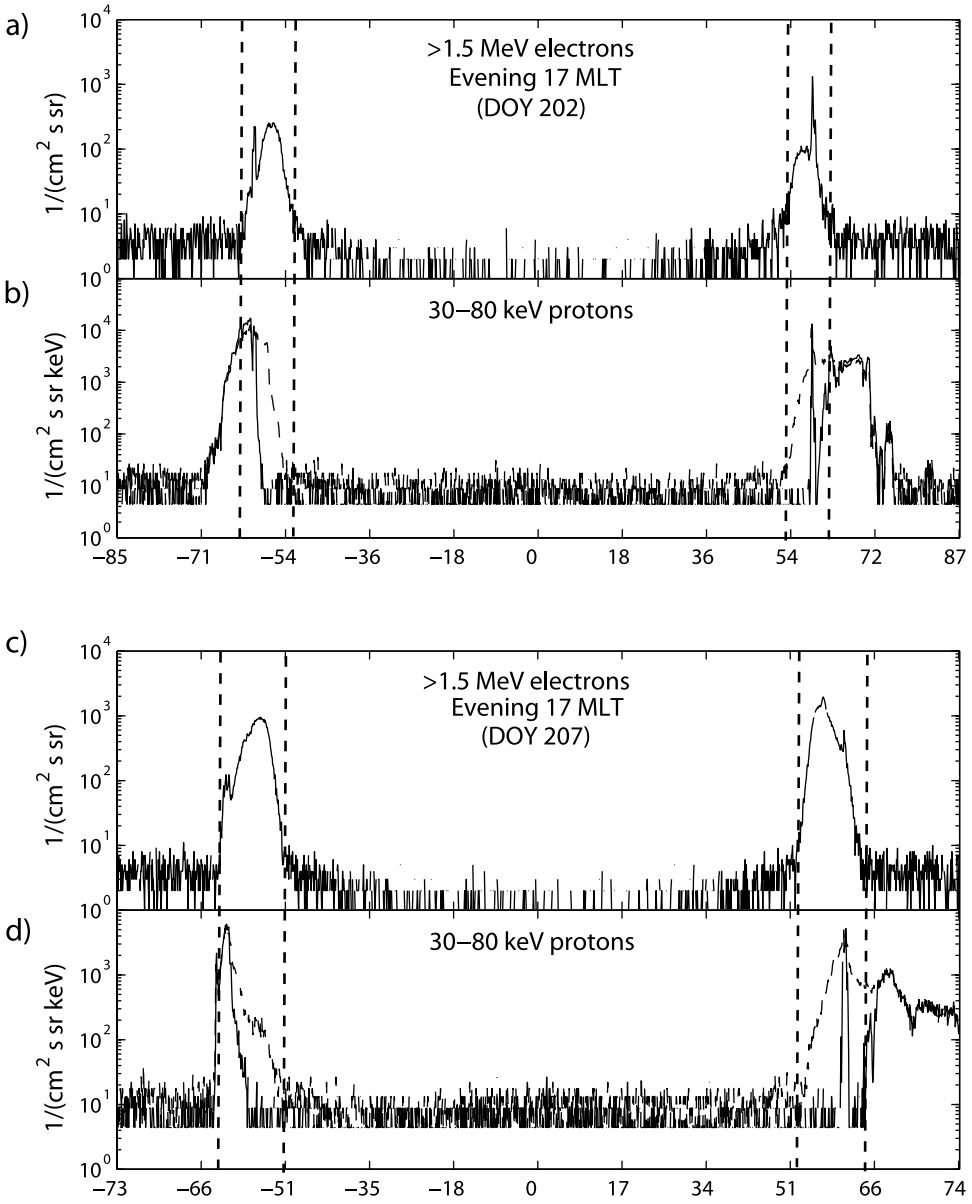

Figure 4. Particle data from NOAA-12 on 21 and 26 July 1998. The figure exhibits electrons >1.5 MeV and protons 30–80 keV, from the 90deg (dashed line) and 0deg detectors (a and b) from an eveningside pole-to-pole orbit on 21 July (1215–1305 UT) and (c and d) from an eveningside pole-to-pole orbit on 26 July (0700–0751 UT).

which is indicated by the two black lines, copied from Figure 5c.

[20] Figure 6 shows how electrons with energies >30, >100, >300 keV and 1.5 MeV relate to the solar wind speed, the interplanetary magnetic field B_z component, and the ground-based Dst index. We have selected data from the region $4 < L < 5$ in a MLT range around 0700 and from restricted geographic longitudes. This has been done in order to sample the particle data at a constant magnetic field $B = 3 * 10^{-5}$ *T*. The data from Figures 6d, 6e, and 6f are from both the vertical (solid line) and horizontal (dashed line) MEPED detector, which, at the satellite's position, measures respectively inside and at the edge of the atmospheric loss cone. Notice that fluxes observed by the horizontal (right scale) and vertical detector (left scale) are different. The storm is, as mentioned, associated with a high-speed solar wind stream >700 km/s. B_z exhibits large scale oscillations, and the AE index (not shown here) has elevated values over a prolonged time interval. The relativistic electrons (Figure 6c) start to appear in the recovery phase, and their intensity increases throughout this phase. This is also evident from Figure 5d. The intensity of the >300 keV electrons (Figure 6d) increases at the beginning of day 205 and reaches its highest value in the recovery phase of the storm. The vertical detector shows that there are significant scattering of electrons all the way to the center of the loss cone even if it is a factor of 100 less than at the edge of the loss cone. The temporal behavior of the >300 keV electrons

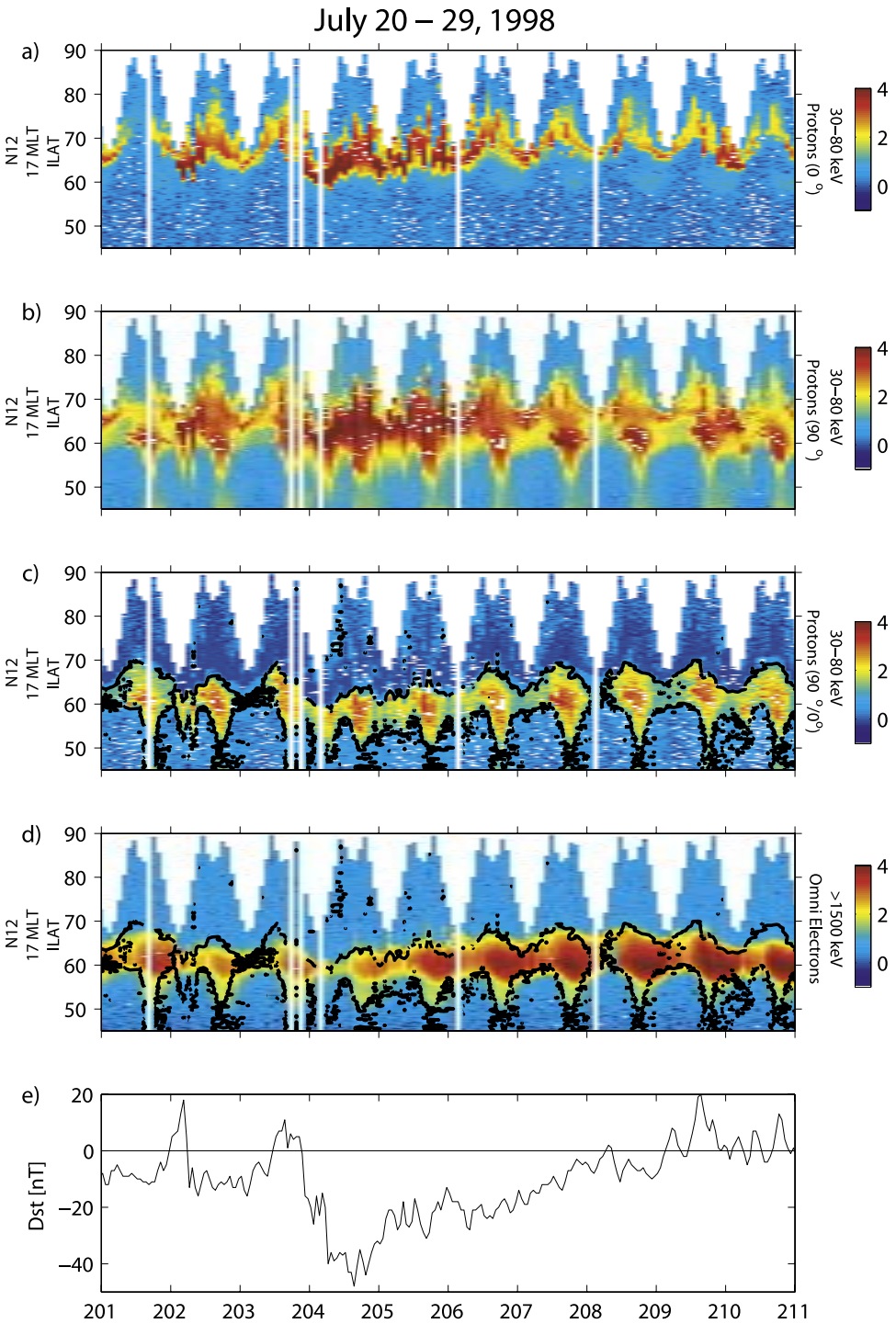

Figure 5. (a and b) The 30–80 keV precipitating and mirroring protons detected with NOAA-12 in the evening sector (1700 MLT). The flux (cm^{-2} sr^{-1} s^{-1} keV^{-1}) is shown with a logarithmic color scale, plotted versus ILAT and UT time. Also shown is (c) the ratio of locally mirroring protons over precipitating protons. The green, yellow, and red region represents the area where the flux of locally mirroring protons is much higher than the flux of precipitating protons (the anisotropic proton zone). Also shown is (d) relativistic electrons where the contour of the anisotropic proton zone is plotted in black and (e) the Dst index.

resemble that of the >1.5 MeV electrons. The intensity of the >100 keV electrons (Figure 6e) has a more abrupt increase in the main phase of the storm, and the intensity stays constant during the recovery phase. The >30 keV electrons are most intense in the main phase and early recovery phase of the storm. In the recovery phase (day 206), the >30 keV electron intensity starts to decrease rapidly. In contrast to that, the >300 keV and >1.5 MeV electrons exhibit increasing inten-

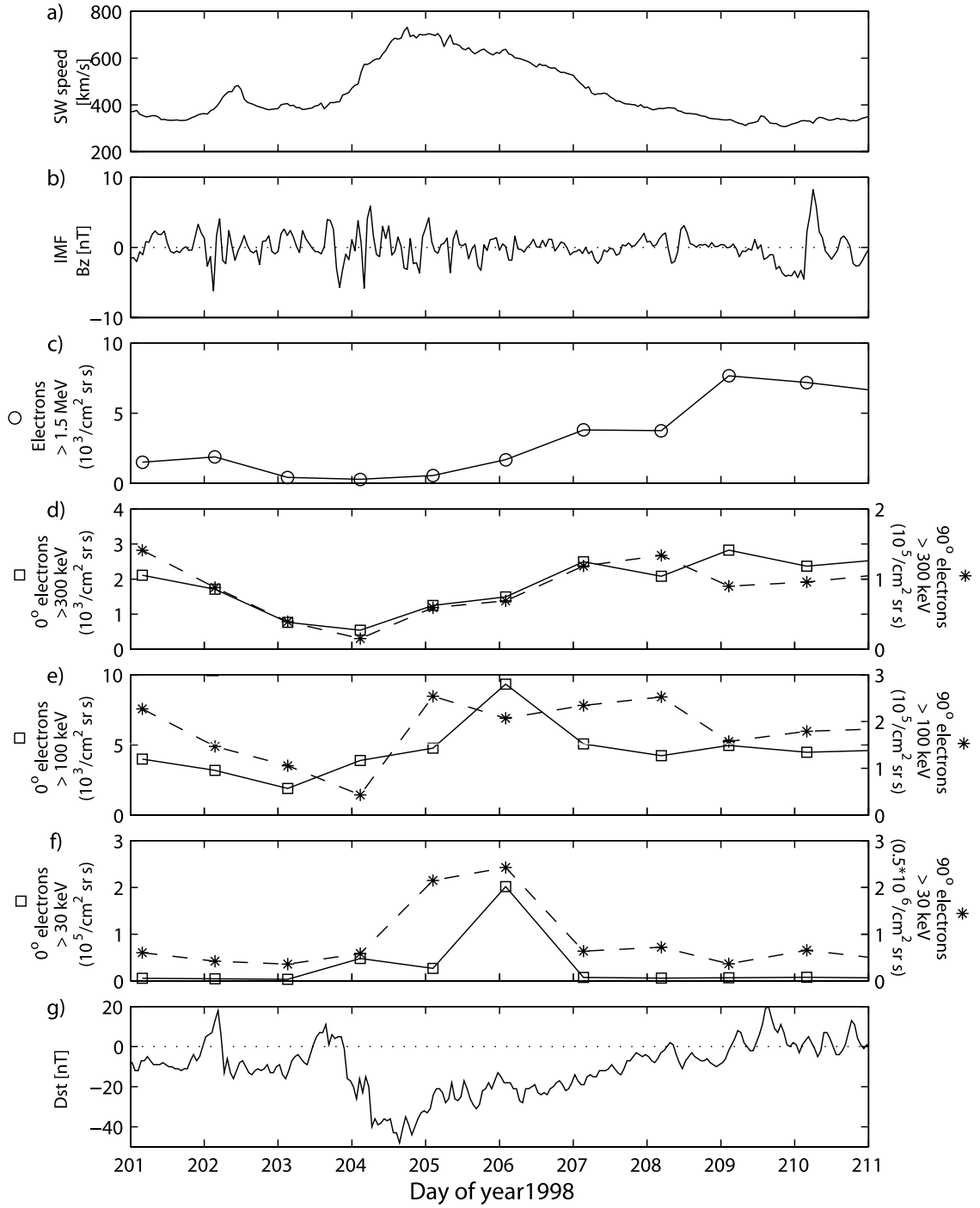

Figure 6. (a and b) The solar wind speed and the IMF B_z component and the flux of (c) >1.5 MeV, (d) >300 keV, (e) >100 keV, and (f) >30 keV electrons observed between $4 < L < 5$. Figure 6c displays fluxes observed by the dome detector, while Figures 6d, 6e, and 6f display fluxes observed by the vertical (solid line) and the horizontal (dashed line) MEPED detector. In Figures 6d–6f the solid lines have their axis to the left and the dashed lines their axis to the right. Notice that the flux observed by the horizontal and vertical detector have different scales. The observations are done at constant magnetic field strength ($B = 3 * 10^{-5}$ T) at 0700 MLT. Also shown is (g) the Dst index.

sity throughout the storm recovery phase, and support the theory [e.g., *Summers et al.*, 1998] that the >30 keV and >100 keV electron populations could function as seeds for the relativistic electrons and for the generation of chorus waves. Observations at MLT 0300, 1400, and 1700 show very similar behavior as the one at MLT 0700.

5. Summary and Discussions

[21] The proton precipitation typically consist of two regions: (1) the isotropic poleward zone, which on the nightside is due to the nonadiabatic pitch angle scattering of protons connected to the field line curvature of the stretched magnetic field line in the magnetotail [e.g., *Sergeev et al.*, 1983], and (2) the anisotropic zone where the trapped population prevails. The anisotropic zone is equatorward of the isotropy boundary and exists at all local times, while the isotropic zone is most prominent in the midnight/evening local time sector. In the isotropic zone the ring current protons are stable to wave growth. In the anisotropic zone, however, the protons are unstable and can generate wave growth. *Thorne and Kennel* [1971], *Fraser and Nguyen* [2001], and *Loto'aniu et al.* [2006] have established that EMIC waves generated by an unstable proton population can precipitate relativistic electrons in the ~1 MeV range.

[22] **Our Observations Show**

[23] 1. Peaks and structures in the relativistic electron precipitation match peaks and structures in the anisotropic proton flux. This shows a close relationship between precipitating relativistic electrons and unstable protons. *Lundblad and Søraas* [1978] and *Yahnina et al.* [2000] observed bursts of protons inside the anisotropic proton zone. *Lundblad and Søraas* [1978] found the proton precipitation spikes to be closely related to SAR arcs and *Yahnina et al.* [2000] found a connection between the spikes and Pc1 pulsations on the ground, which are believed to be EMIC waves generated by the ion-cyclotron instability of energetic ring current protons at the equator. The spikes are thus the particle counterparts of the EMIC waves [*Titova et al.*, 1998; *Yahnina et al.*, 2003]. The pitch angle distribution within the spikes vary from moderate to strong as shown in Figures 2–3 and Figure 4, respectively. The strength of the scattering in these localized areas will depend on the conditions for EMIC wave-particle interaction (plasmapause, plumes). The regions with enhanced loss of relativistic electrons and protons can be observed at all local times.

[24] 2. The loss of relativistic electrons is not restricted to a narrow region just at/or inside the plasmapause. *Thorne and Kennel* [1971] suggested that the MeV electron precipitation region should be restricted to a narrow zone just within the plasmapause. We believe that weak pitch angle diffusion by EMIC waves growing on unstable anisotropic proton populations are precipitating relativistic electrons inside the whole anisotropic proton zone. This agrees, for example, with *Joselyn and Lyons* [1976], *Williams et al.* [1976], *Hu and Fraser* [1994], and *Fraser and Nguyen* [2001], who showed that EMIC waves could interact with protons in a wide *L*-range. *Joselyn and Lyons* [1976] have shown that the proton population is able to generate EMIC waves in the *L*-region 3.5–7. *Williams et al.* [1976] suggested the region from 2.5–5 Earth radii to be unstable to ion cyclotron waves due to hot ring current plasma in the recovery phase. These regions are more or less coincident with the anisotropic proton zone observed by low-altitude polar-orbiting satellites. *Fraser and Nguyen* [2001] used CRRES data and found that EMIC waves occurred both inside and outside the plasmasphere, and the number of events occurring outside the plasmasphere was even greater. Our observations show that precipitation of relativistic electrons due to weak pitch angle scattering takes place throughout the whole region where the pitch angle distribution of the protons is unstable to the growth of the ion-cyclotron waves.

[25] 3. EMIC wave-particle interactions scatter relativistic electrons not only in the evening/noon MLT sector but within the whole region of anisotropic proton flux, irrespective of the local time. This conclusion is based on the fact that relativistic electrons are confined to the region of anisotropic proton flux for all four MLT sectors considered. *Anderson* [1996] also found EMIC waves to exist at other local times than evening/noon sector, although with varying intensity.

[26] 4. EMIC waves scatter relativistic electrons into the atmospheric loss cone, throughout the prolonged recovery phase of the geomagnetic storm. During this phase of the storm there is a buildup of the relativistic electrons and a decrease in the >100 keV electrons. These observations suggest that the >30 keV and >100 keV electrons can act as seed particles for a high-energy electron buildup during the storm recovery phase. This is in accord with theory; for example, *Summers et al.* [1998] showed that whistler-mode waves are effective at accelerating electrons from energies near 100 keV to above 1 MeV in the region outside the plasmapause during a storm recovery phase. *Summers et al.* [2004] further showed that enhanced whistler-mode chorus waves generated during prolonged substorm activity could generate MeV electron flux increases in the outer radiation zone. This provides an increasing flux of relativistic electrons in the outer radiation belt due to whistler-mode chorus, at the same time as EMIC wave-particle interactions remove relativistic electrons from the radiation belt and scatter them into the atmospheric loss cone.

6. Conclusions

[27] The whole anisotropic proton zone is a region suitable for pitch angle scattering due to EMIC wave-particle interactions. Relativistic electrons experience weak pitch angle scattering within this region independent of local time. The EMIC wave-particle interactions are thus not restricted to a narrow region at/or inside the plasmapause nor are the EMIC wave-particle interactions restricted to the evening/noon MLT sector. The EMIC waves at the plasmapause and plumes are very strong and more easy to observe than the weaker EMIC waves in the anisotropic proton zone.

[28] Peaks and structures in the relativistic electron precipitation match peaks and structures in the anisotropic proton flux. Some localized areas have optimal conditions for EMIC wave-particle interactions, such as the plasmapause and plumes, and these areas will then have particularly strong pitch angle diffusion, which in turn will give precipitation spikes of relativistic electrons and protons. Collocated precipitation spikes of relativistic electrons and anisotropic protons are found at all local times. These spikes

are connected to Pc1 pulsations on the ground and thereby particle counterparts of EMIC waves in the equatorial plane.

[29] In a particular calculation, *Albert* [2003] found that EMIC waves only operate on MeV electrons with equatorial pitch angles below 30deg. Locally mirroring particles at the altitude of the NOAA-12 spacecraft has equatorial pitch angles around 6deg at L = 4 or 60deg ILAT and thus well inside the region where EMIC waves operate. The recent study by *Shprits et al.* [2006b] indicates that EMIC wave scattering, which is very effective near the loss cone, may be the dominant loss mechanism and can control the loss rate of MeV electrons. Other waves, like chorus and hiss, are efficient in scattering relativistic electrons with large equatorial pitch angles toward the loss cone where the EMIC waves bring them into the loss cone. The close spatial correspondence we have found between the precipitation of relativistic electrons and the anisotropic proton flux suggests that ion-cyclotron waves generated by the ring current protons could certainly be the dominant loss mechanism for the relativistic electrons.

[30] We conclude that relativistic electrons precipitate within the whole anisotropic proton zone due to weak pitch angle scattering, and the precipitation spikes are due to strong pitch angle scattering possibly connected with increased plasma density. The >30 keV and >100 keV electrons decrease as the relativistic electrons increase during the storm recovery phase. This supports the theory that low-energy particles function as seed particles for the high-energy buildup during the storm recovery phase.

[31] **Acknowledgments.** We thank Danny Summers for comments and fruitful discussions and the Norwegian Research Council for financial support to the Space Research program, project 147652/V30. M. Sandanger thanks the University of Bergen for her research grant and M. Sørbø for graphic support. We acknowledge M. S. Greer for software and graphic work. We also acknowledge the World Data Center for Geomagnetism, Kyoto, for providing the Dst index and the ACE team for providing solar wind data.

[32] Zuyin Pu thanks Yuri Shprits and another reviewer for their assistance in evaluating this paper.

References

Albert, J. M. (2003), Evaluation of quasi-linear diffusion coefficients for EMIC waves in a multispecies plasma, *J. Geophys. Res.*, *108*(A6), 1249, doi:10.1029/2002JA009792.

Anderson, B. J. (1996), Recent observations of electromagnetic ion cyclotron waves in space, *Adv. Space Res.*, *17*(10), 1041–1050.

Cornwall, J. M., F. V. Coroniti, and R. M. Thorne (1971), Unified theory of SAR arc formation at the plasmapause, *J. Geophys. Res.*, *76*(19), 4428–4445.

Engebretson, M. J., A. Keiling, K.-H. Fornacon, C. A. Cattell, J. R. Johnson, J. L. Posch, S. R. Quick, K.-H. Glassmeier, G. K. Parks, and H. Rème (2007), Cluster observations of Pc 1–2 waves and associated ion distributions during the October and November 2003 magnetic storms, *Planet. Space Sci.*, *55*, 829–848.

Fraser, B. J., and T. S. Nguyen (2001), Is the plasmapause a preferred source region of electromagnetic ion cyclotron waves in the magnetosphere?, *J. Atmos. Sol. Terr. Phys.*, *63*, 1225–1247.

Friedel, R. H. W., G. D. Reeves, and T. Obara (2002), Relativistic electron dynamics in the inner magnetosphere - A review, *J. Atmos. Sol. Terr. Phys.*, *64*, 265–282.

Horne, R. B., and R. M. Thorne (1998), Potential waves for relativistic electron scattering and stochastic acceleration during magnetic storms, *Geophys. Res. Lett.*, *25*(15), 3011–3014.

Horne, R. B., S. A. Glauert, and R. M. Thorne (2003), Resonant diffusion of radiation belt electrons by whistler-mode chorus, *Geophys. Res. Lett.*, *30*(9), 1493, doi:10.1029/2003GL016963.

Horne, R. B., R. M. Thorne, S. A. Glauert, J. M. Albert, N. P. Meredith, and R. R. Anderson (2005a), Timescale for radiation belt electron acceleration by whistler mode chorus waves, *J. Geophys. Res.*, *110*, A03225, doi:10.1029/2004JA010811.

Horne, R. B., et al. (2005b), Wave acceleration of electrons in the Van Allen radiation belts, *Nature*, *437*(8), doi:10.1038/nature03939.

Horne, R. B., et al. (2006), Mechanisms for the acceleration of radiation belt electrons, in *Recurrent Magnetic Storms: Corotating Solar Wind Streams*, *Geophys. Monogr. Ser.*, vol. 167, edited by B. T. Tsurutani et al., 151–173, AGU, Washington, D. C.

Hu, Y. D., and B. J. Fraser (1994), Electromagnetic ion cyclotron wave amplification and source regions in the magnetosphere, *J. Geophys. Res.*, *99*(A1), 263–272.

Jordanova, V. K., L. M. Kistler, J. U. Kozyra, G. V. Khazanov, and A. F. Nagy (1996), Collisional loss of ring current ions, *J. Geophys. Res.*, *101*(A1), 111–126.

Joselyn, J. A., and L. R. Lyons (1976), Ion cyclotron wave growth calculated from satellite observations of the proton ring current during storm recovery, *J. Geophys. Res.*, *81*(13), 2275–2282.

Li, X., and M. A. Temerin (2001), The electron radiation belt, *Space Sci. Rev.*, *95*, 569–580.

Loto'aniu, T. M., R. M. Thorne, B. J. Fraser, and D. Summers (2006), Estimating realtivistic electron pitch angle scattering rates using properties of electromagnetic ion cyclotron wave spectrum, *J. Geophys. Res.*, *111*, A04220, doi:10.1029/2005JA011452.

Lundblad, J. A., and F. Søraas (1978), Proton observations supporting the ion cyclotron wave theory of SAR arc formation, *Planet. Space Sci.*, *26*, 245–254.

Lyons, L. R., and R. M. Thorne (1972), Parasitic pitch angle diffusion of radiation belt particles by ion-cyclotron waves, *J. Geophys. Res.*, *77*(28), 5608–5616.

Meredith, N. P., R. M. Thorne, R. B. Horne, D. Summers, B. J. Fraser, and R. R. Anderson (2003a), Statistical analysis of relativistic electron energies for cyclotron resonance with EMIC waves observed on CRRES, *J. Geophys. Res.*, *108*(A6), 1250, doi:10.1029/2002JA009700.

Meredith, N. P., M. Cain, R. B. Horne, R. M. Thorne, D. Summers, and R. R. Anderson (2003b), Evidence for chorus-driven electron acceleration to relativistic energies from a survey of geomagnetically disturbed periods, *J. Geophys. Res.*, *108*(A6), 1248, doi:10.1029/2002JA009764.

Raben, V. J., D. S. Evans, H. H. Sauer, S. R. Sahm, and M. Huynh (1995), TIROS/NOAA Satellite Space Environment Monitor data archive documentation: 1995 update, *Tech. Memo. ERL SEL-86*, NOAA, Silver Spring, Md.

Reeves, G. D., K. L. McAdams, R. H. W. Friedel, and T. P. O'Brien (2003), Acceleration and loss of relativistic electrons during geomagnetic storms, *Geophys. Res. Lett.*, *30*(10), 1529, doi:10.1029/2002GL016513.

Sandanger, M. I., F. Søraas, K. Aarsnes, K. Oksavik, D. S. Evans, and M. S. Greer (2005), Proton injections into the ring current associated with B_z variations during HILDCAA events, in *The Inner Magnetosphere: Physics and Modeling*, *Geophys. Monogr. Ser.*, vol. 155, edited by T. I. Pulkkinen, N. A. Tsyganenko, and R. H. W. Friedel, pp. 249–255, AGU, Washington, D. C.

Sergeev, V. A., E. M. Sazhina, N. A. Tsyganenko, F. J. A. Lundblad, and F. Søraas (1983), Pitch-angle scattering of energetic protons in the magnetotail current sheet as the dominant source of their isotropic precipitation into the nightside ionosphere, *Planet. Space Sci.*, *31*(10), 1147–1155.

Shprits, Y. Y., R. M. Thorne, R. B. Horne, S. A. Glauert, M. Cartwright, C. T. Russel, D. N. Baker, and S. G. Kanekal (2006a), Acceleration mechanism responsible for the formation of the new radiation belt during the 2003 Halloween solar storm, *Geophys. Res. Lett.*, *33*, L05104, doi:10.1029/2005GL024256.

Shprits, Y. Y., W. Li, and R. M. Thorne (2006b), Controlling effect of the pitch-angle scattering rates near the edge of the loss cone on electron lifetimes., *J. Geophys. Res.*, *111*, A12206, doi:10.1029/2006JA011758.

Søraas, F., J. A. Lundblad, N. F. Maltseva, V. Troitskaya, and V. Selivanov (1980), A comparison between simultaneous I.P.D.P. groundbased observations and observations of energetic protons obtained by satellites, *Planet. Space Sci.*, *28*, 387–405.

Søraas, F., K. Aarsnes, J. Å. Lundblad, and D. S. Evans (1999), Enhanched pitch angle scattering of protons at mid-latitudes during geomagnetic storms, *Phys. Chem. Earth C*, *24*(1–3), 287–292.

Søraas, F., K. Aarsnes, K. Oksavik, and D. S. Evans (2002), Ring current intensity estimated from low-altitude proton observations, *J. Geophys. Res.*, *107*(A7), 1149, doi:10.1029/2001JA000123.

Søraas, F., K. Aarsnes, K. Oksavik, M. I. Sandanger, D. S. Evans, and M. S. Greer (2004), Evidence for particle injection as the cause of Dst reduction during HILDCAA events, *J. Atmos. Sol. Terr. Phys.*, *66*, 177–186.

Søraas, F., K. Aarsnes, D. V. Carlsen, K. Oksavik, and D. S. Evans (2005), Ring current behavior as revealed by energetic proton precipitation, in *The Inner Magnetosphere: Physics and Modeling*, *Geophys. Monogr. Ser.*, vol. 155, edited by T. I. Pulkkinen, N. A. Tsyganenko, and R. H. W. Friedel, pp. 237–247, AGU, Washington, D. C.

Summers, D., and C. Ma (2000), A model for generating relativistic electrons in the Earth's inner magnetosphere based on gyroresonant wave-particle interactions, *J. Geophys. Res.*, *105*(A2), 2625–2639.

Summers, D., and R. M. Thorne (2003), Relativistic electron pitch-angle scattering by electromagnetic ion cyclotron waves during geomagnetic storms, *J. Geophys. Res.*, *108*(A4), 1143, doi:10.1029/2002JA009489.

Summers, D., R. M. Thorne, and F. Xiao (1998), Relativistic theory of wave-particle resonant diffusion with application to electron acceleration in the magnetosphere, *J. Geophys. Res.*, *103*(A9), 20,487–20,500.

Summers, D., C. Ma, N. P. Meredith, R. B. Horne, R. M. Thorne, and R. R. Anderson (2004), Modeling outer-zone relativistic electron response to whistler-mode chorus activity during substorms, *J. Atmos. Sol. Terr. Phys.*, *66*, 133–146.

Thorne, R. M., and C. F. Kennel (1971), Relativistic electron precipitation during magnetic storm main phase, *J. Geophys. Res.*, *76*(19), 4446–4453.

Titova, E. E., et al. (1998), Strong localized variations of the low-altitude energetic electron fluxes in the evening sector near the plasmapause, *Ann. Geophys.*, *16*, 25–33.

Tsurutani, B. T., and W. D. Gonzalez (1987), The cause of high intensity long duration continuous AE activity (HILDCAA's): Interplanetary Alfvén waves trains, *Planet. Space Sci.*, *35*, 405–412.

Yahnina, T. A., A. G. Yahnin, J. Kangas, and J. Manninen (2000), Proton precipitation related to Pc1 pulsations, *Geophys. Res. Lett.*, *27*(21), 3575–3578.

Yahnina, T. A., A. G. Yahnin, J. Kangas, J. Manninen, D. S. Evans, A. G. Demekhov, V. Y. Trakhtengerts, M. F. Thomsen, G. D. Reeves, and B. B. Gvozdevsky (2003), Energetic particle counterparts for geomagnetic pulsations of Pc1 and IPDP types, *Ann. Geophys.*, *21*, 2281–2292.

Williams, D. J., G. Hernandez, and L. R. Lyons (1976), Simultaneous observations of the proton ring current and stable auroral red arcs, *J. Geophys. Res.*, *81*(4), 608–616.

K. Aarsnes, M. Sandanger, and F. Søraas, Department of Physics and Technology, University of Bergen, Allégt 55, N-5007 Bergen, Norway. (marit.sandanger@ift.uib.no)

D. S. Evans, NOAA Space Environment Center, 325 Broadway, Boulder, CO 80305, USA.

K. Oksavik, Johns Hopkins University Applied Physics Laboratory, 11100 Johns Hopkins Road, Laurel, MD 20723, USA.